INSTITUTE OF PHYSICS PUBLISHING COMBUSTION THEORY AND MODELLING

Combust. Theory Modelling **8** (2004) 593–606 PII: S1364-7830(04)71644-7

Investigation of the transition from lightly sooting towards heavily sooting co-flow ethylene diffusion flames

M D Smooke[1], R J Hall[2], M B Colket[2,4], J Fielding[3], M B Long[1], C S McEnally[1] and L D Pfefferle[1]

[1] Center for Combustion Studies, Yale University, New Haven, CT, USA
[2] United Technologies Research Center, East Hartford, CT, USA
[3] Mercer Oliver Wyman, New York, NY, USA

Received 10 November 2003, in final form 5 May 2004
Published 11 June 2004
Online at stacks.iop.org/CTM/8/593
doi:10.1088/1364-7830/8/3/009

Abstract

Laminar, sooting, ethylene-fuelled, co-flow diffusion flames at atmospheric pressure have been studied experimentally and theoretically as a function of fuel dilution by inert nitrogen. The flames have been investigated experimentally using a combination of laser diagnostics and thermocouple-gas sampling probe measurements. Numerical simulations have been based on a fully coupled solution of the flow conservation equations, gas-phase species conservation equations with complex chemistry and the dynamical equations for soot spheroid growth. Predicted flame heights, temperatures and the important soot growth species, acetylene, are in good agreement with experiment. Benzene simulations are less satisfactory and are significantly under-predicted at low dilution levels of ethylene. As ethylene dilution is decreased and soot levels increase, the experimental maximum in soot moves from the flame centreline toward the wings of the flame. Simulations of the soot field show similar trends with decreasing dilution of the fuel and predicted peak soot levels are in reasonable agreement with the data. Computations are also presented for modifications to the model that include: (i) use of a more comprehensive chemical kinetics model; (ii) a revised inception model; (iii) a maximum size limit to the primary particle size; and (iv) estimates of radiative optical thickness corrections to computed flame temperatures.

1. Introduction

Combustion-generated soot particles from land-based sources pose a significant health risk and are the subject of stringent new EPA regulations. In addition, soot contributes to thermal

[4] Author to whom any correspondence should be addressed.

radiation loads on combustor liners and turbine blades. Soot emissions also enhance contrail formation and tactical visibility of aircraft. A quantitative understanding of the soot growth and oxidation mechanism and the ability to model these processes are critical to the development of strategies to control emissions.

In earlier numerical simulations of soot distributions in diluted methane and ethylene co-flow diffusion flames [1, 2], predictions in the annular layer just inside the flame's wings compared well with experiments. However, predictions along the centreline were noticeably under-predicted (by a factor of two to three). In the flames of both fuel types, the experimental soot profiles peaked along (or near) the centreline but model predictions put the soot peaks in the wings. The simulations of Kennedy *et al* [3] for an undiluted, heavily sooting flame [4] were characterized by similar results for centreline soot levels (factor of 10 under-prediction), with quantitative agreement in the annular regions. Alternatively, Kaplan *et al* [5] presented results that agreed well, at least qualitatively, with the experiments. The available experimental evidence suggested a tendency for 'non-sooting' flames to produce soot most strongly along the centreline, with flames nearer the smoking point having the most soot off-axis in the wings inside the flame. While varying the diluent level is an established method of varying soot production in diffusion flames [6, 7], there have been limited studies of the centreline to wing shift in soot profiles that occurs with dilution. The challenge this poses for soot models has led to the experimental and theoretical investigations described here on dilution effects in ethylene co-flow flames.

By studying a series of diffusion flames, which are varied from non-sooting (defined as no soot emitting from the flame) towards sooting conditions (with soot emitting from the flame) with a fully coupled soot formation model [1, 2], and by sequentially reducing the fuel diluent, we are able to develop an enhanced understanding of the factors controlling the localization of soot in co-flow diffusion flames. In the next two sections we discuss the experimental methodology and the numerical procedure used to compute the flame structure. The details of the soot model followed by a section on the results of the study complete the paper.

2. Experimental approach

The details of the burner and diagnostic approaches are similar to those described in [2]. Atmospheric pressure, over-ventilated, axisymmetric, co-flowing, non-premixed laminar flames were generated with a burner in which the fuel flows from an uncooled 4.0 mm inner diameter vertical brass tube (wall thickness 0.38 mm). The oxidizer flows from the annular region between this tube and a 50 mm diameter concentric tube. The oxidizer was air while the fuel was a mixture containing ethylene and nitrogen. The fuel and oxidizer flow velocities are $35\,\mathrm{cm\,s^{-1}}$. Electronic mass flow controllers accurate to within 5% governed fuel flow rates. The same burner apparatus was used for all the experiments. The temperature of the brass tube for this slightly lifted flame was less than 330 K. In addition to the flame previously investigated [2] with the central fuel tube feed with 32% ethylene and the remainder nitrogen, three new flames were investigated in this study. For these new flames, experimental inlet conditions were matched except that the fuel dilution levels were changed to 40%, 60%, and 80% ethylene.

Probe measurement procedures have been described previously [8, 9]. Gas temperatures were measured with 75 μm wire-diameter Type R thermocouples and corrected for radiation heat transfer effects using standard techniques [8]. A rapid insertion procedure was used to minimize errors due to soot deposition onto the thermocouple. The absolute uncertainty of these measurements is estimated to be ± 100 K and the relative uncertainty to be ± 10 K.

At 2000 K, the radiation correction is computed to be 140 K for the spherical junctions used in this study. We estimate that the uncertainty in the use of the proper Nusselt number for heat transfer and possible catalytic effects contribute at least half the uncertainty in the cited temperatures [10]. Species concentrations were measured by extracting gas samples from the flames with a narrow-tipped quartz microprobe and analysing these samples with on-line mass spectrometry [9].

The soot volume fraction field is determined by laser-induced incandescence (LII). At sufficient laser intensities, the LII signal has been shown to be directly proportional to the soot volume fraction [11]. The fundamental of an Nd : YAG laser (1064 nm) is expanded and focused into a sheet 10 mm high with a beam waist of approximately 0.3 mm. Laser energy is maintained around 9 mJ/pulse to provide a laser fluence $\sim 3 \times 10^7\,\mathrm{W\,cm^{-2}}$. Only the centre 5 mm of the laser sheet is used to maintain constant intensity across the imaged section. Incandescence and scattered light are collected perpendicular to the laser axis with a camera objective, passed through a coloured glass filter (Corning 2–60) and focused onto an image intensifier, which is lens-coupled to a CCD camera. The intensifier is gated for 1 μs centred on the laser pulse. Although it has been shown that a prompt 50 ns gate would result in less error in volume fraction measurement for a change in particle diameter [12], the time response of the intensifier gating may cause greater problems. The intensifier used in these experiments has $\sim$50 ns rise and fall times and shorter gate times could result in an inconsistency in the measurements. Therefore, the signal is acquired over the entire LII signal when the intensifier is fully 'on'. In the region of greatest incandescence signal, a survey is conducted of incandescence signal versus laser intensity to maximize signal intensity without saturation (e.g. soot destruction) at any point in the flow field. One hundred images are acquired of both single-pulse LII and flame luminosity at 5 mm increments along the vertical axis. The raw LII images are averaged and corrected for luminosity and optical throughput to generate composite soot volume fraction images. Thermocouple particle densitometry (TPD) measurements of volume fraction discussed in [2] are used for calibration.

3. Computational approach

The axisymmetric computational model [1, 2] employs the gas-phase diffusion flame equations in the velocity–vorticity formulation with buoyancy and the particle sectional approach presented in [13]. The result is a strongly coupled set of elliptic partial differential equations. The gas and soot equations are additionally coupled through non-adiabatic radiative loss in the optically thin approximation. Radial and axial velocities, the vorticity, the temperature, the gas-phase species, and the particle sectional mass fractions are computed. The chemical mechanism was derived from one of the more comprehensive and well-validated sets available for ethylene [14]. Modifications included elimination of a few species identified to be relatively unimportant to the soot-forming processes as well as an enhancement by a factor of 2.5 times the rate constants for propargyl recombination (to form both phenyl + H and benzene) and a factor of five reduction in the rate for $C_3H_3 + H \Leftrightarrow C_3H_2 + H_2$. The modified rate constants were selected based on a reaction path analysis in order to increase the predicted benzene concentrations by about a factor of two. (Even with these modifications, predicted benzene levels are still significantly below experimental levels.) The resultant mechanism contains 476 reactions and 66 chemical species. Twenty soot sections are included in the formulation. The result is a model that requires a total of 90 dependent variables to be solved at each grid point. The system is closed with the ideal gas law and appropriate boundary conditions

are applied on each side of the computational domain. Local properties are evaluated via transport and chemistry libraries. The sectional thermophoretic velocities in the free molecule regime are given in [13] as are the sectional diffusion velocities written with a mass-weighted mean diffusion coefficient for each size class. The governing conservation equations are solved on a two-dimensional mesh by combining a Newton-based steady-state and a time-dependent solution method [15]. A time-dependent solution is first obtained on a coarse grid and then grid points are inserted adaptively to increase the resolution in regions of high spatial activity.

4. Soot modelling

4.1. Inception

The soot inception model employed builds upon our earlier formulation [13] of naphthalene production rates. Quasi-steady-state concentrations of intermediate polycyclic aromatic hydrocarbons (PAHs) are assumed to exist and are attained rapidly. In this proposed model, instead of the presumption that naphthalene and phenanthrene lead directly to inception, steady-state expressions have been derived for the formation of a high molecular weight condensed PAH. The model is based on the sequence of growing naphthalenyl to pyrenyl through sequential acetylene addition, H-atom elimination, H-atom abstraction and acetylene addition followed by ring closure. Overall, the reaction can be written as $C_{10}H_7 + 3C_2H_2 \Leftrightarrow C_{16}H_9 + 2H + H_2$. This sequence is assumed to continue to form yet larger PAH structures with the overall balance of $C_{10}H_7 + 3nC_2H_2 \Leftrightarrow C_{10+2n}H_{7+2n} + 2nH + nH_2$. Limitations to the use of this expression are related to (i) uncertainties in the side reactions that may remove critical intermediate species and (ii) the time it takes to achieve steady-state concentration levels. Utilization of this approximate reaction sequence for inception prevents coalescence for small particle sizes. This approach has provided better simulations of the experimental data. The computed soot results are relatively independent of the number, n, taken to be 21 in this work. In general, smaller values of $n = 8$–10 are recommended to simulate PAH–PAH interactions for high molecular weight PAH. The inception rate expression given in [13] was heuristically multiplied by a factor of two for these studies. Scrubbing of gas-phase species by inception was neglected since the kinetic models utilized in this study under-predict benzene mole fractions by upwards of a factor of two (see also [2]).

4.2. Surface growth

The surface growth model used in the numerical simulations was based on the premixed flame data of Harris–Weiner [16] where we assumed an activation energy of $E_s = 31.8\,\text{kcal mol}^{-1}$ [17] (see also [1, 2]). In addition, we have performed computations using the 'MODFW' surface growth mechanism as described by [18], using an expression as corrected by [18] and referred to as the 'CH' model. Results are incomplete but appear to be quantitatively similar to computations using the Harris–Weiner model. This 'CH' model was shown to be critical in modelling soot growth in high temperature flames [20] and is similar to that proposed as the HACA model by [21].

4.3. Particle dynamics

The growth of soot particles is modelled as a classical aerosol dynamics problem, involving the division of the size range of interest into discrete intervals or classes with a logarithmic

Table 1. Comparison of selected experimental and computational results.

% Ethylene (mass)	32%		40%		60%		80%	
	Expt	Model	Expt	Model	Expt	Model	Expt	Model
Flame height (cm)	2.7	2.8	3.2	3.3	5.0	5.2	7.1	7.1
Peak temperature (K)	2084	1973	2130	2005	2199	2054	Too hot	2081
Peak CL temp (K)	2040	1918	2078	1884	1970	1765	1823	1682
Peak soot (ppm)	1.0	1.1	2.5	2.0	6.0	4.3	18	6.5
Peak CL soot/Pk soot	1.0	1.0	1.0	0.8	0.59	0.48	0.44	0.28
Peak acetylene (%)	3.7	3.23	3.5	3.7	4.3	4.4	4.9	4.74
Peak benzene (ppm)	160	211	330	275	630	359	1000	355
Power loss (Rad/Hcomb)		0.15		0.18		0.25		0.30

transformation of the size range [22]. The application of this approach to soot modelling is described in [13]. The contributions from the inception processes are incorporated in the first sectional bin, whose lower mass boundary is set equal to the mass of the smallest inception species. Cases were run with the number of soot sections ranging from 9 to 25. No significant differences were observed in the predicted soot fields due to increases in the number of soot sections. For all work reported here, 20 soot sections have been used.

The spherical particle sectional model used here normally imposes no constraint on the final particle size, and does not account for aggregate formation. Coalescence, as assumed in our model, destroys particle surface area, whereas aggregation, to the first order, does not. An approximate treatment of aggregate formation effects on surface area is employed by setting coalescence and surface growth rates to zero for particles beyond a critical input diameter (25 nm is suggested from experiments, and this is the value we used in the model). Coalescence is still allowed for smaller diameter particle–particle collisions and hence particles larger than the maximum diameter can still be formed in the simulations. Particles with sizes significantly larger than 25 nm can be viewed as aggregated particles with multiple individual spheroids; this is, however, a highly approximate treatment of large particle morphology. Oxidation of soot by O_2 and OH is treated as described in [1, 2].

Note that the sectional analysis has the virtue that it is, in principle, not limited to spherical particles. Adding equations for the average number of primary spheroids within a section would make it possible to model more accurately the formation of soot aggregates [23, 24], but this is beyond the scope of this paper.

4.4. Radiative power loss

In the optically thin approximation employed in this study, the power radiated from soot and gas bands (CO_2, H_2O, and CO, using the exponential wideband model) is computed using the expressions in [25]. A more sophisticated analysis to assess the importance of optical thickness or radiative re-absorption effects was also performed in this work. Details of the procedure are provided below.

5. Results

Features of the flame studied previously [2] and the three flames investigated in this study are shown in table 1. Attempts to examine an undiluted flame (100% ethylene in the fuel tube) were made; however, experiments exhibited flow instabilities and simulations had convergence difficulties.

Table 1 compares experiments and our modelling results for flame heights (the axial location at which the peak temperature reaches a maximum along the centreline), peak temperatures, peak centreline (CL) temperatures, peak soot volume fractions and peak concentrations of selected species. In addition, the ratio of the peak centreline soot volume fraction to the peak flame soot volume fraction is provided. Results reported in table 1 indicate excellent overall comparisons of peak soot concentrations and the peak centreline to peak flame soot ratio for the 32% and 40% flames with good to reasonable comparison for the 60% and 80% flames, respectively.

Comparisons of two-dimensional colour contours between the experimental and computational results show that the flame model simulates the main features of the flame and the changes in the flame structure as the ethylene dilution is decreased. A comparison of the experimental and computed contours for the 60% diluted flame is provided in figure 1. As concluded previously [2], the high experimental temperatures very low in the flame near the centreline (<1 cm) are a result of limitations, e.g. conductive heat transfer along the support wires, in the experimental method at these locations rather than early preheating of the fuel. The results clearly demonstrate that, on a global level, the structures of the flames are reproduced well. Figure 2 shows temperature as a function of height, along the centreline for the four flames in this study. The model reproduces the rapid rise in temperature at heights of 1.0–2.5 cm; but the computations do not adequately approach or attain the peak centreline temperatures. Also shown in figure 2 is the centreline profile for the 80% ethylene case in which radiation is ignored. Non-adiabatic radiative loss (primarily from gas-band radiation) drastically modifies the temperature profile, and lengthens the flame by about 15%. Comparison of the computed temperature with experimental data suggests that the optically thin model overestimates radiation losses. Optical thickness effects might contribute to the over-prediction and are discussed later in the paper.

Acetylene is a principal surface growth species and also contributes to inception. Hence, accurate simulation of acetylene is also critical to predictions of soot. As shown in figure 3, centreline acetylene profiles are simulated well and the changes with decreasing dilution are also reproduced, although concentrations are under-predicted at low heights. The model for the 32% ethylene flame reproduces benzene concentrations along the centreline reasonably, but as depicted in figure 4, significant increases in benzene observed experimentally with decreasing dilution are not simulated well and are spatially displaced. The under-prediction of benzene (trend with increasing fuel concentration) can be expected to affect predicted soot concentrations. Presumably, these low benzene predictions are directly linked to the low temperature predictions in this portion of the flame.

The experimental decay in benzene occurs rapidly and at temperatures too low for thermal decomposition, at least at the temperatures computed by the model. The rapid benzene loss may be caused by rapid removal through interactions with larger aromatic species or soot. The under-predicted temperatures may inhibit faster growth rates lower in the flame and under-predict rapid thermal decomposition rates higher in the flame. The dramatic changes in the benzene and acetylene profiles, when radiation losses are not included (see figures 3 and 4), demonstrate this effect.

Two principal deficiencies of the soot model used in [2] were that (i) centreline soot was always substantially under-predicted and (ii) the computed wings of the flame were extended much beyond those determined by experiment. The original model allowed particles to continue to coalesce and grow to form primary particles that were more than a factor of two above the maximum experimental values ($\sim$25 nm). Large diameter soot particles slowed the oxidation process and were the direct cause of the extended wings. Recognizing that soot particles reach a maximum primary size in experiments, the soot dynamics model was

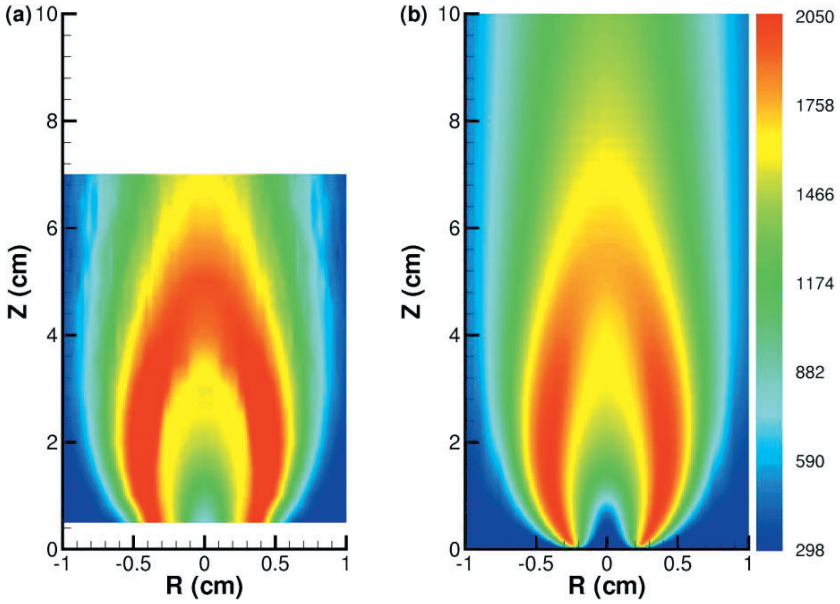

Figure 1. Experimental (*a*) and computed (*b*) two-dimensional colour contour plots of temperature for the 60% ethylene flame.

modified to cease both coalescence and surface growth above a cut-off particle size. With this modification, primary particle size was limited and the extended wings were eliminated. In this application, particles of a certain size range and above (mid-range of this size class was 25 nm) will not coalesce with particles of comparable or larger sizes. Note that growth of particles to sizes above this cut-off size still occurs in the model due to coalescence involving smaller particles.

Experimental soot volume fractions for the 32%, 40%, 60% and 80% flames are compared to the computed solutions in figure 5. The experiments depict a dramatic shift in the location of maximum soot away from the centreline to the wings as ethylene is increased. The model, though it under-predicts the peak soot levels, agrees qualitatively with this trend. The dilute flame (32%) has a temperature profile that peaks on the centreline, with soot forming below the flame front and peaking on the centreline. As the ethylene flow increases, the temperature peaks off the centreline; soot is formed inside the flame front and grows along the full length of the flame, confined by thermophoretic forces. Thus, as the flame lengthens with decreased levels of dilution, soot levels in the wings increase substantially due both to the increased residence time and to the increased levels of (experimental) benzene. As discussed previously, uncertainties in the predictions of benzene and temperature contribute to inaccuracies in the quantitative prediction of soot along the centreline with decreasing dilution of the fuel, but the qualitative trend is predicted.

The sensitivity of predicted soot levels to the inception rate is such that the factor of two enhancement of inception discussed previously has given rise to 40–50% increases in soot for the richer flames. Higher soot levels increase radiative losses, and the peak centreline temperatures decrease significantly (up to 75 K).

Evaluation of the radiative loss (optically thin) using predicted temperatures, soot volume fractions and radiating species concentrations leads to the predicted radiative loss (radiative

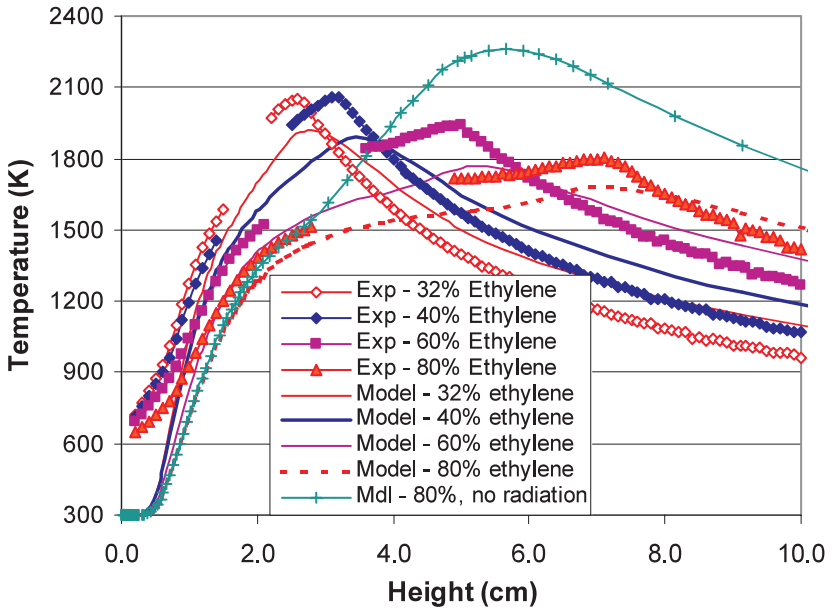

Figure 2. Comparison of predicted and experimental centreline temperatures as a function of height for the 32%, 40%, 60% and 80% ethylene flames (radiation-free solution for the 80% flame is also included).

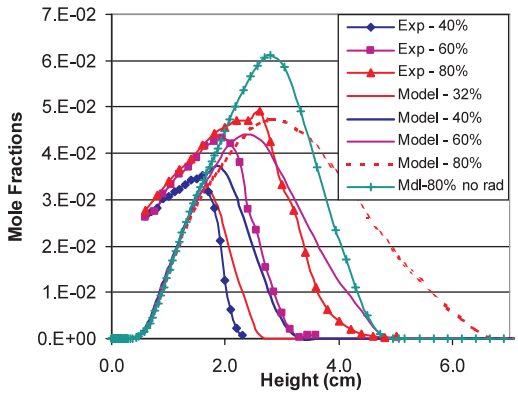

Figure 3. Comparison of the computed and experimental centreline concentrations of acetylene.

loss/heat of combustion) percentages shown in table 1. For the 80% ethylene case, the integrated loss over the total flame volume is predicted to be 28–30% of the flame enthalpy release, of which gas band radiation alone accounts for about 18%. The increase in radiative loss with decreasing dilution of ethylene is a result of both the increase in residence time and soot volume fraction and contributes to the substantial reduction in peak flame temperatures (see table 1). If the model properly predicted larger soot volume fraction f_v along the centreline (as observed experimentally), we would expect an even larger relative contribution of soot to the radiation loss, as well as increased effects on optical re-absorption.

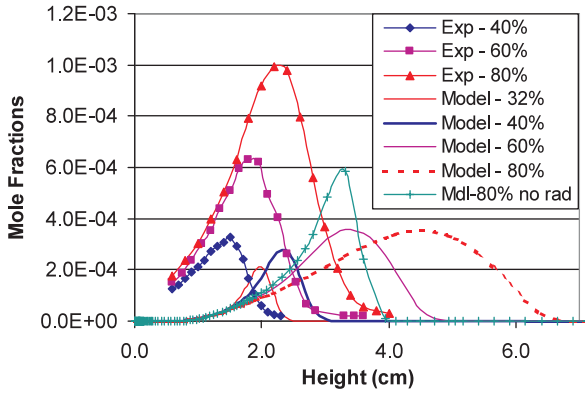

Figure 4. Comparison of the computed and experimental centreline concentrations of benzene.

5.1. Optical thickness corrections

Low calculated temperatures, as have been observed in these investigations, could be caused by overestimation of radiative loss. In principle, some re-absorption of thermal emissions can occur, particularly on or near the centreline, which receives emissions from surrounding regions of the flame. This optical thickness effect reduces the net rate of thermal radiation energy loss. To test whether this effect might be the cause of our under-predictions of temperature along the centreline, more complex calculations of the local net emission rate including re-absorption were undertaken.

The calculation used the 'discrete transfer' method of Lockwood and Shah [26]. The algorithm directs rays into the interior of the flame from all calculation boundary surfaces assuming a vacuum boundary condition. For these calculations, 400 rays emanating from each boundary point were nominally used—a number at which the calculations had lost sensitivity to the number of rays. The path of each ray is registered, and then a line-of-sight, path-integrated calculation of radiative flux is performed using RADCAL, a narrow-band radiation model that includes both gas and soot emissions and allows for path inhomogeneities [27]. The algorithm produces the spectrally integrated radiative flux divergence, which is the local emission rate minus re-absorption effects. Fuel emission–absorption effects were not included. Because the narrow-band calculation is very time consuming, it was not directly integrated into the energy conservation equation solution. Rather, an iterative procedure was used in which converged temperatures and species concentrations from the standard optically thin calculation were input to the RADCAL solution, providing a net radiative emission term, which was then used as a fixed sink rate in the energy equation. The soot absorption coefficient in the optically thin model was set equal to that used in RADCAL, and the integrated intensity of the CO_2 4.3 μm band (exponential wide band model) was set at a value which ensured local gas band emission rates comparable to RADCAL. The procedure was repeated until the process converged.

For the 60% ethylene flame, the optical thickness corrections were large enough to increase temperatures along the centreline in the early soot formation zone by as much as 40 K. The higher temperatures lead to increased peak soot levels of about 15%. As shown in figure 6(*a*), re-absorption leads to higher temperatures along the centreline lower in the flame, but these higher temperatures and the increased soot lead to increased radiative emission higher in the flame, and a lower peak temperature there. The reader is reminded that the high experimental temperatures at the burner exit are artefacts of the experimental technique [2]. The calculated effect on benzene is seen to be significant, as shown in figure 6(*b*).

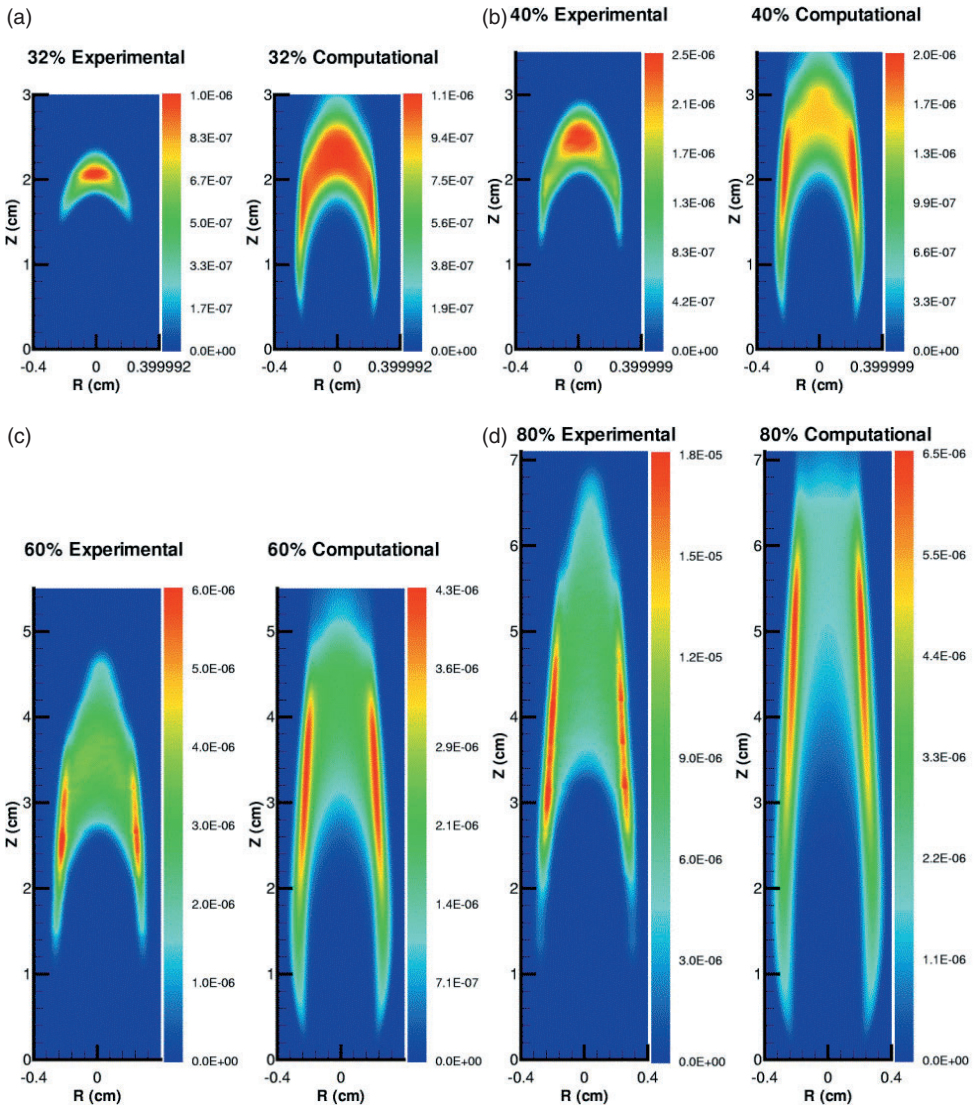

Figure 5. Experimental and computed soot contours for the (*a*) 32%, (*b*) 40%, (*c*) 60% and (*d*) 80% ethylene flames.

Comparisons of soot volume fractions for the experiments, for the computations using the original optically thin assumption, and for the computations with the radiative re-absorption effects are shown in figures 7(*a*)–(*c*) for the 40%, 60% and 80% ethylene flames. As can be observed, computations with the re-absorption effects consistently improve the predicted soot structure within the flame. The very significant improvement can also be inferred form the peak centreline-to-peak soot ratios and the peak centreline soot levels. The (Pk CL Soot/Pk Soot) ratios for the 40%, 60% and 80% dilution flames are 94%, 63% and 45%, respectively, when re-absorption effects were included and the (peak soot) volume fractions were 2.1, 5.8 and 7.0 ppm. Except for the peak soot in the 80% flame, both these sets of values agree very well with the experimental determinations (see table 1) and are noticeably improved from the

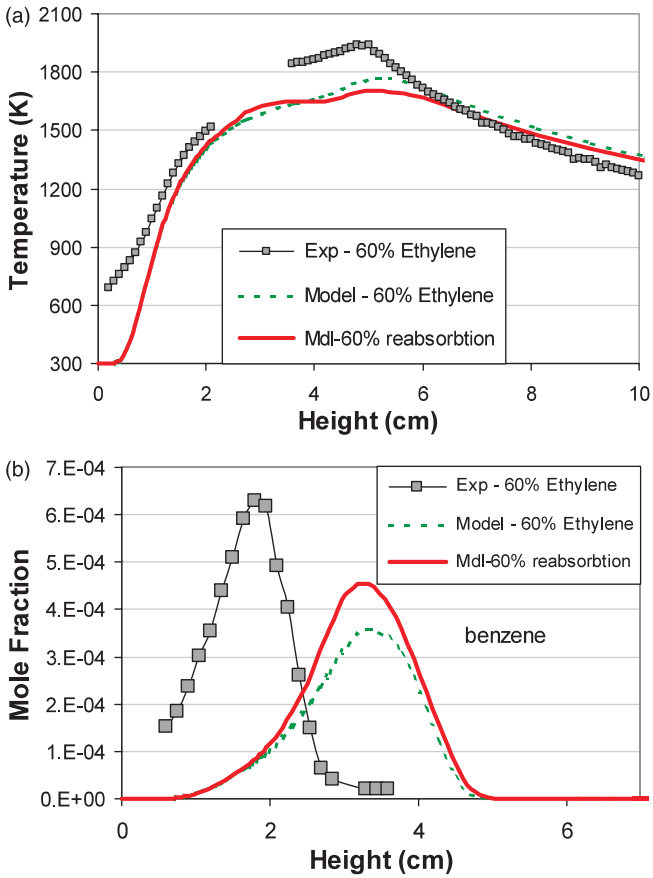

Figure 6. (*a*) Effect of radiative re-absorption on centreline temperature for the 60% flame, (*b*) effect of radiative re-absorption on centreline benzene for the 60% flame.

model results utilizing the optically thin assumption. We conclude that optical thickness effects are important for accurate calculations, but only partially explain the discrepancies between experimental and theoretical temperatures and benzene concentrations.

5.2. Alternative chemical mechanism and soot growth model

Calculations have also been performed using the chemical and soot growth mechanisms of Appel *et al* [28]. Their chemical mechanism is an expanded version of that used in our base model, and leads to the production of pyrene (A4). In the Appel *et al* soot model, dimerization of A4 provides the nucleation rate. Surface growth occurs via a six-step acetylene-based HACA mechanism, and provision is made for surface growth from PAH (A4) addition. These particle growth rates have been incorporated into the sectional algorithm, together with consistent coalescence and oxidation rates.

Figure 8 compares the predictions of three model calculations using (a) the present chemical kinetics and soot growth models, (b) the Appel *et al* chemical mechanism and present soot growth models and (c) the Appel *et al* chemical kinetics and the Appel *et al* soot growth mechanism. For this set of figures, note that each panel is colour-scaled to its own maximum soot level. As seen from a comparison of (a) and (b), there is little net effect

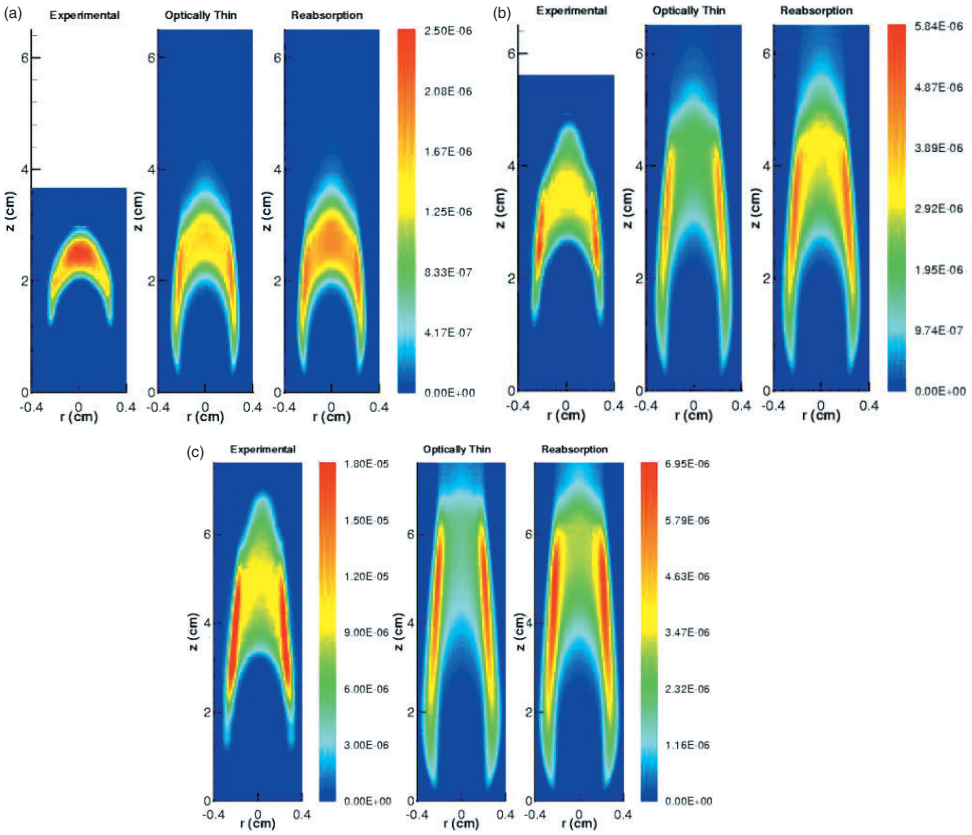

Figure 7. Comparison of experimental two-dimensional contours of soot volume fractions with computations based upon both the optically thin assumption and optical re-absorption for the (*a*) 40%, (*b*) 60% and (*c*) 80% ethylene co-flow flames.

of the different gas-phase chemical kinetics on soot production. There are small differences in predicted acetylene and benzene with the former values 10% higher and the latter smaller by 25% compared with the Appel *et al* kinetics mechanism. These contrary effects probably counterbalance each other in the soot predictions when the same soot kinetics are used. We also point out that the acetylene peaks at a position slightly higher (2 mm) with the Appel kinetics, while the benzene peaks a little lower (by about 4 mm). The Appel *et al* benzene profile, although quantitatively lower, provides a slightly better spatial agreement with the experiment. However, with the fully coupled Appel *et al* gas-phase kinetics and soot inception/growth model (c), soot predictions are significantly different. This model produces a soot profile in which the peak soot occurs along the centreline and the quantitative agreement is poorer (peak soot is only 0.75 ppm) than in the (a) or (b) calculations (compare figure 5 and table 1). Additional work remains in comparing and contrasting these two models.

6. Conclusions

Laminar, sooting, ethylene-fuelled, co-flow diffusion flames have been studied experimentally and theoretically as a function of ethylene dilution. Flame parameters important to prediction of soot concentrations have been measured, and the experiments pose a very stringent test for

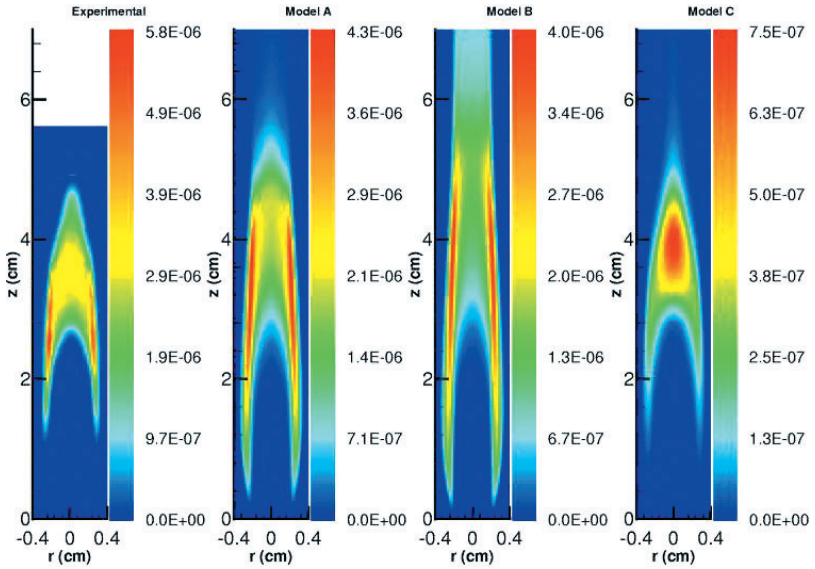

Figure 8. Comparison of chemical and soot growth mechanisms for the 60% flame. Model A = base chemical and soot growth mechanisms; model B = Appel *et al* [28] chemical and base soot growth mechanisms; model C = Appel *et al* chemical and soot growth mechanisms.

assessment of chemical and soot kinetics mechanisms. Predicted flame heights, temperatures and acetylene are in excellent to good agreement with experiment. Experimentally, soot profiles obtained from laser-induced soot incandescence (LII) undergo a shift away from peaking on the flame centreline towards the wings of the flame as the sooting level increases. Theoretical simulations agree qualitatively with this observation. Specifically, as the ethylene flow increases, the temperature peaks off the centreline; soot is formed inside the flame front and grows along the full length of the flame, confined by thermophoretic forces. Thus, as the flame lengthens with decreased levels of dilution, soot levels in the wings increase substantially due both to the increased residence time and to the increased levels of benzene. Modifications to the soot model, including (i) termination of surface growth and coalescence at a predetermined diameter (e.g. about 25 nm), (ii) use of a more comprehensive reaction model and (iii) simulation of large molecular weight PAHs for inception have been investigated. Agreement with the experimental data set is good. Centreline temperatures, benzene concentrations and soot volume fractions are progressively under-predicted as dilution levels decrease. Rapid (experimental) benzene decay in the soot-forming regime suggests the possibility that nascent soot particles are actively scrubbing the benzene from the flame.

The results of this study confirm the importance of correct predictions of temperatures and benzene concentrations to the ability to predict accurately the distribution and magnitude of soot volume fractions. Discrepancies in the benzene and soot profiles may in part be due to low predicted temperatures, incompleteness in the kinetics/soot models or experimental uncertainty. Reduction in uncertainties in the experimental measurements, particularly when using intrusive methods, could be the subject of a future study. The simulations show the strong coupling of radiative power loss to soot formation and the necessity of including them in computations. Optical thickness corrections have been estimated through detailed calculations to be significant, especially for the high ethylene dilution flames (60–80% ethylene). Optical re-absorption, temperature and soot production are strongly coupled, and have complex interactions in the flame. Re-absorption arising from both gas bands

and soot raises local temperatures, increasing soot production. These elevated soot levels can then give rise to enhanced radiative cooling higher in the flame. Furthermore, this analysis demonstrates that radiative re-absorption is at least a partial contributor to the theory–experiment discrepancies. Use of an alternative chemical/soot growth mechanism does not resolve the remaining discrepancies.

Acknowledgments

The authors acknowledge support from the Air Force Office of Scientific Research (Dr Julian Tishkoff, contract monitor) and the DOE Office of Basic Energy Sciences (Dr Frank Tully, contract monitor) for support of this work under contracts F49620-98-C-0008 and DE-FG02-88ER13966, respectively. One of the authors has been partially supported by the Strategic Environmental Research and Development Program (SERDP) under a contract coordinated by Dr Don Phelps of the Air Force Research Laboratories (Wright-Patterson AFB). We are also grateful to Mr Brian Dobbins for his assistance in the preparation of the figures.

References

[1] Smooke M D, McEnally C S, Pfefferle L D, Hall R J and Colket M B 1997 *Combust. Flame* **117** 117
[2] McEnally C S, Schaffer A M, Long M B, Pfefferle L D, Smooke M D, Colket M B and Hall R J 1998 *Proc. Combust. Inst.* vol 27 (Pittsburgh: The Combustion Institute) p 1497
[3] Kennedy I M, Rapp D R, Santoro R J and Yam C 1996 *Combust. Flame* **107** 386
[4] Santoro R J, Semerjian H G and Dobbins R A 1983 *Combust. Flame* **51** 203
[5] Kaplan C R, Shaddix C R and Smyth K C 1996 *Combust. Flame* **106** 392
[6] Kent J H and Wagner H Gg 1984 *Proc. Combust. Inst.* vol 20 (Pittsburgh: The Combustion Institute) p 1007
[7] Boedeker L R and Dobbs G M 1986 *Combust. Sci. Technol.* **46** 301
[8] McEnally C S, Köylü Ü Ö, Pfefferle L D and Rosner D E 1997 *Combust. Flame* **109** 701
[9] McEnally C S and Pfefferle L D 1996 *Combust. Sci. Technol.* **116–117** 183
[10] Shaddix C R 1999 *Proc. 33rd Natl Heat Transfer Conf. HTD99-282 (Albuquerque, NM, 15–19 August)*
[11] Quay B, Lee T-W, Ni T and Santoro R J 1994 *Combust. Flame* **97** 384
[12] Mewes B and Seitzman J M 1997 *Appl. Opt.* **36** 709
[13] Hall R J, Smooke M D and Colket M B 1997 *Physical and Chemical Aspects of Combustion: A Tribute to Irvin Glassman* ed R F Sawyer and F L Dryer (*Combustion Science and Technology Book Series*) (London: Gordon and Breach)
[14] Sun C J, Sung C J, Wang H and Law C K 1996 *Combust. Flame* **107** 321, a copy of the modified mechanism is available on request (colketmb@utrc.utc.com)
[15] Smooke M D, Ern A, Tanoff M A, Valdati B A, Mohammed R K, Marran D F and Long M B 1996 *Proc. Combust. Inst.* vol 26 (Pittsburgh: The Combustion Institute) p 2161
[16] Harris S J and Weiner A M 1983 *Combust. Sci. Technol*. **31** 155
[17] Hura H S and Glassman I 1988 *Proc. Combust. Inst.* vol 22 (Pittsburgh: The Combustion Institute) p 371
[18] Colket M B and Hall R J 1994 *Soot Formation in Combustion Mechanisms and Models* ed H Bockhorn (*Springer Series in Chemical Physics* vol 59) (Berlin: Springer) p 442
[19] Xu F, Sunderland P B and Faeth G M 1997 *Combust. Flame* **108** 471
[20] Smooke M D, Yetter R A, Parr T P, Hanson-Parr D M, Tanoff M A, Colket M B and Hall R J 2000 *Proc. Combust. Inst.* vol 28 (Pittsburgh: The Combustion Institute) p 2013
[21] Frenklach M and Wang H 1990 *Proc. Combust. Inst.* vol 23 (Pittsburgh: The Combustion Institute) p 1559
[22] Gelbard F and Seinfeld J H 1980 *J. Coll. Int. Sci.* **78** 485
[23] Rogak S N 1991 *PhD Dissertation* Cal. Tech.
[24] Rogak S N 1997 *Aerosol Sci. Technol.* **26** 127
[25] Hall R J 1994 *J. Quant. Spectrosc. Radiat. Transfer* **51** 635
[26] Lockwood F C and Shah N G 1981 *Proc. Combust. Inst.* vol 18 (Pittsburgh: The Combustion Institute) p 1405
[27] Grosshandler W L 1993 RADCAL: a narrow-band model for radiation calculations in a combustion environment *NIST Technical Note* 1402
[28] Appel J, Bockhorn H and Frenklach M 2000 *Combust. Flame* **121** 122, www.me.berkeley.edu-soot-codes.f